

Normal-Incidence InAs Self-Assembled Quantum-Dot Infrared Photodetectors With a High Detectivity

Zhengmao Ye, Joe C. Campbell, Zhonghui Chen, Eui-Tae Kim, and Anupam Madhukar

Abstract—An InAs/AlGaAs quantum-dot infrared photodetector based on bound-to-bound intraband transitions in undoped InAs quantum dots is reported. AlGaAs blocking layers were employed to achieve low dark current. The photoresponse peaked at $6.2\ \mu\text{m}$. At 77 K and $-0.7\ \text{V}$ bias, the responsivity was $14\ \text{mA/W}$ and the detectivity, D^* , was $10^{10}\ \text{cm}\cdot\text{Hz}^{1/2}/\text{W}$.

MID- and far-infrared ($3\text{--}20\ \mu\text{m}$) detection is a key technology for numerous commercial, military and space applications, e.g., night vision, thermal imaging, chemical analysis, nondestructive detection, remote sensing, and missile guidance and defense. Due to the long carrier capture and relaxation times, quantum-dot infrared photodetectors (QDIPs) have the potential for lower dark current and higher photoresponse than quantum-well infrared photodetectors (QWIPs). Most importantly, the three-dimensional (3-D) confinement of electrons in the quantum dots permits QDIPs to operate in the normal incidence mode, unlike QWIPs which are not sensitive to radiation that is incident perpendicular to the quantum wells [1]. To date, there have been several papers on InAs/GaAs, InGaAs/GaAs, and InGaAs/InGaP QDIPs [2]–[11]. Most of the devices employed a doped active region, which resulted in high dark current. In this paper, we report an InAs/GaAs QDIP with unintentionally doped active region and AlGaAs barrier layers. Our previous study on QDIPs with doped active region (~ 2 electrons per quantum dot) show that the dark current is higher than QDIPs with an unintentionally doped active region. The AlGaAs layers act as blocking layers [6]–[11] for dark current, as first demonstrated in [6]. The devices reported here have demonstrated low dark current, low noise, and high detectivity.

The InAs QDIP studied in this work belongs to the class of n-i-n structure QDIPs (Fig. 1) [6]–[8]. The samples were grown on semi-insulating GaAs (001) substrates by solid-source molecular beam epitaxy. Five layers of 3-monolayer (ML) InAs quantum dots were inserted between highly Si-doped top and bottom GaAs contact layers. The punctuated island growth technique was used to grow the quantum dots [12]. The GaAs spacer layers between the contact layers and the nearest quantum-dot layer had a thickness of 219–239 ML. 30-ML GaAs regions

Manuscript received November 20, 2001; revised May 31, 2002. This work was supported by AFOSR under the MURI program.

Z. Ye and J. C. Campbell are with Microelectronics Research Center, University of Texas at Austin, Austin, TX 78712 USA (e-mail: zmye@mail.utexas.edu).

Z. Chen, E.-T. Kim, and A. Madhukar are with the Department of Materials Science and Physics, University of Southern California, Los Angeles, CA 90089 USA.

Publisher Item Identifier 10.1109/JQE.2002.802159.

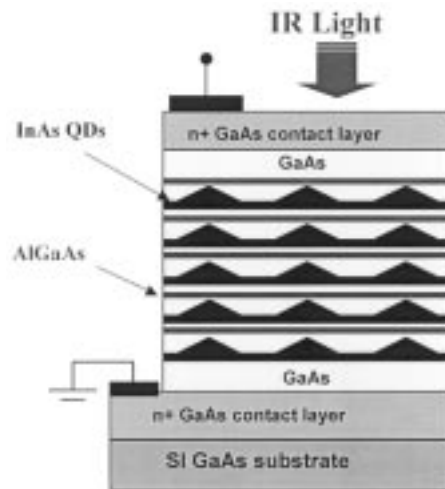


Fig. 1. Schematic of InAs/GaAs QDIP structure.

were used as the quantum-dot cap layers. In order to reduce the dark current, four pairs of AlAs/GaAs (1 ML/4 ML) were introduced below the quantum-dot layers and on the top of the GaAs cap layers. The size of the pyramidal-shaped quantum dots was estimated with atomic force microscopy (AFM) and a cross-sectional transmission electron microscope (XTEM): the height was $59\pm 17\ \text{\AA}$ and the base width was $210\ \text{\AA}$. The dot density was $625\pm 40/\mu\text{m}^2$.

Device fabrication followed standard procedure: photolithography, wet chemical etching, metal deposition and lift-off, and rapid thermal annealing. Mesas having a diameter of $250\ \mu\text{m}$ and a height of $\sim 1.4\ \mu\text{m}$ were defined with an etch of $\text{H}_3\text{PO}_4:\text{H}_2\text{O}_2:\text{LH}_2\text{O}$ (8:1:61). A $50\text{-}\mu\text{m}$ -diameter top contact and the bottom contact were formed by evaporation and liftoff of Au/Ni/AuGe. The contacts were then annealed at $430\ \text{^\circ C}$ for 20 s. In the following discussion, “positive” bias means that a positive voltage was applied to the top contact.

The normal-incidence spectral response was measured with a Nicolet Magna-IR 570 Fourier transform infrared (FTIR) spectrometer and an SRS 570 low-noise current preamplifier. Fig. 2 shows the spectral response at 0.8-V bias and at temperatures of 63 K, 77 K, and 100 K. The intraband photoresponse peaks occurred at $6.2\ \mu\text{m}$ for all three spectra. The full-width at half-maximum (FWHM) of the spectrum, $\Delta\lambda$, was $\sim 0.4\ \mu\text{m}$, from which it follows that $\Delta\lambda/\lambda = 7.5\%$. The narrow spectral width is consistent with our previous results [8], [13]. These results indicate that the electron transitions are intraband transitions from

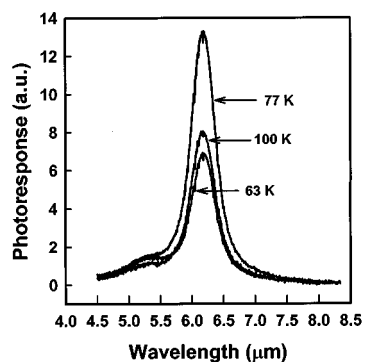


Fig. 2. Normal incident photoresponse of the QDIP sample at the bias of 0.8 V and temperatures of 63 K, 77 K, and 100 K.

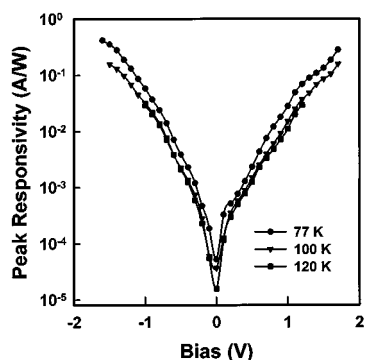


Fig. 3. Peak responsivity at 77 K, 100 K, and 120 K.

a lower bound state to a higher bound state [13]. The observed spectral width reflects the uniformity of the size of the quantum dots. The QDIP exhibits the highest photoresponse at 77 K. This can be explained as follows. As the temperature increases, more electrons occupy the lower states of the quantum dots. As long as there are unoccupied excited states available, the electrons in the lower states can participate in photon induced intraband transitions. However, a further increase in the number of electrons in the quantum dots, which results from the increase in dark current at higher temperature, will cause a decrease in the number of unoccupied excited states and, consequently, a decrease in the photoresponse. Additionally, a decrease in photo-excited electron lifetime at higher temperature can also result in a decrease in the photoresponse.

The absolute spectral responsivity was calibrated with a blackbody source ($T = 995$ K). Since the blackbody spectrum included near infrared radiation, which could result in interband transitions, in addition to mid- and long-wavelength photons, optical filters were placed next to the aperture of the blackbody to block radiation with wavelengths less than $3.5 \mu\text{m}$. Fig. 3 shows the peak spectral responsivity versus bias at temperatures of 77 K, 100 K, and 120 K. With an increase in positive bias, the responsivity increased from 0.33 mA/W at 0.1 V to 280 mA/W at 1.7 V. For negative bias, the responsivity increased near four orders of magnitude from 5.2×10^{-2} mA/W at zero bias to 418 mA/W at -1.6 V. Negative differential responsivity [8] was not observed within the bias range from -1.6 to 1.7 V. The different responsivity curves for the positive and negative bias are attributed to the asymmetric shape of the quantum dots along the growth direction and the wetting layers beneath the

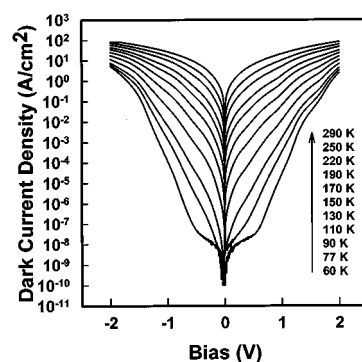


Fig. 4. Dark current density at temperature ranging from 60 K to 296 K.

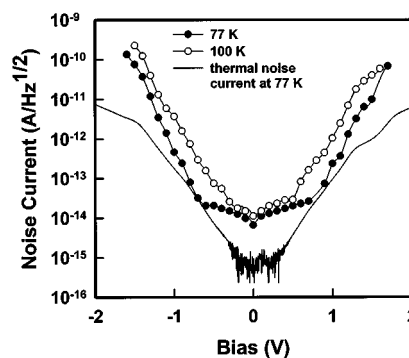


Fig. 5. Measured noise current (dots) at 77 K and 100 K, and calculated thermal noise current at 77 K.

quantum dots. Consequently, electrons in the quantum dots experience different barrier heights, depending on whether transport is toward the top or bottom contacts.

Dark current density versus voltage characteristics are shown in Fig. 4 for temperature in the range from 60 K to 296 K. The structural asymmetry of the quantum dots also results in asymmetrical dark current density for positive and negative bias. At low bias, the increase in dark current density is due to the fact that as the bias increases, more electrons occupy the quantum dots, which results in an increase in the average sheet electron density. When a large fraction of the quantum-dots states are occupied, further increase in bias does not significantly alter the sheet electron density. This causes a lowering of the energy barrier for injected electrons at the contact layers, which results in the nearly exponential increase of the dark current. At 0.7 -V bias, the dark current density was 2.5×10^{-7} A/cm² at 60 K. With increasing temperature, it increased over seven orders of magnitude to 11.1 A/cm² at room temperature. Similarly, at -0.7 -V bias, there was an increase of over eight orders of magnitude from 1.6×10^{-7} A/cm² at 60 K to 14.4 A/cm² at 296 K. Compared to a similar structure without the $\text{Al}_{0.2}\text{Ga}_{0.8}\text{As}$ blocking layers, the dark current has been suppressed by over three orders of magnitude [8]. For bias < 0.7 V and $T > 100$ K, the dark current increased exponentially with temperature, which suggests that in this temperature range, the dark current originates from thermionic emission. The calculated activation energy was 196 meV at zero bias, which was close to the energy corresponding to the cutoff wavelength (193 meV) of the sample. For temperatures lower than 100 K, sequential resonant tunneling and phonon-assisted tunneling are probably the dominant components of the dark current.

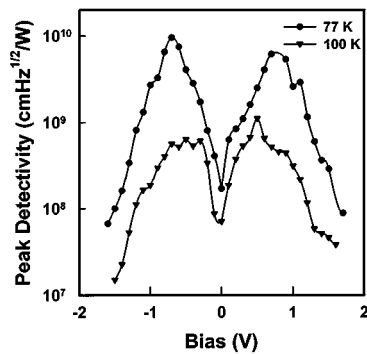


Fig. 6. Peak detectivity at 77 K and 100 K.

The noise current i_n was characterized with low noise current preamplifiers and a SRS 760 fast Fourier transform spectrum analyzer. For $|V_B| > 0.6$ V, the noise current was measured with a SRS current preamplifier. However, below 0.6 V, the photodetector noise current was below the noise floor of the instrument. Near zero bias, a low noise current preamplifier with high gain was used. However, restricted by the input power limitation of this current preamplifier, in the bias range from 0.1 to 0.5 V and -0.5 to -0.1 V, the noise current was interpolated. Fig. 5 shows the noise current of a 250- μm -diameter device at 77 K and 100 K. The calculated thermal noise current I_{th} at 77 K is also shown. The thermal noise current can be expressed as $I_{th} = \sqrt{4kT/R}$, where k is Boltzmann's constant, T is the absolute temperature, and R is the differential resistance of the device, which was extracted from the dark current. At $V_B = -0.7$ V, the calculated thermal noise current (3.2×10^{-14} A/Hz $^{1/2}$) was very close to the measured noise current (2.9×10^{-14} A/Hz $^{1/2}$), which indicates that thermal noise is significant in the low bias region. As the bias was increased, the noise current increased much faster than thermal noise.

The detectivity is given by $D^* = R\sqrt{A \cdot \Delta f}/i_n$, where A is the device area, R is the responsivity, i_n is the noise current, and Δf is the bandwidth. Fig. 6 shows the peak detectivity versus bias at 77 K and 100 K. The best performance was achieved at 77 K and -0.7 V where the peak detectivity was 10^{10} cm·Hz $^{1/2}$ /W. The corresponding responsivity was 14 mA/W. With increase in temperature to 100 K, the peak detectivity dropped to 1.1×10^9 cm·Hz $^{1/2}$ /W at 0.5 V, due to the decrease in responsivity and increase in noise current.

In conclusion, we have demonstrated QDIPs based on bound-to-bound intraband transitions. These QDIPs were sensitive to normal-incident infrared radiation and exhibited a low dark current with $D^* = 9.6 \times 10^9$ cm·Hz $^{1/2}$ /W and $R = 14$ mA/W at -0.7 -V bias and 77 K. In contrast, the QDIPs with the same structure, except with a GaAs barrier layer, exhibited $D^* = 1.5 \times 10^9$ cm·Hz $^{1/2}$ /W at 77 K.

ACKNOWLEDGMENT

The authors would like to thank Dr. J. Beck of the DRS for help with calibration of responsivity and valuable discussions.

REFERENCES

- [1] V. Ryzhii, "The theory of quantum-dot infrared phototransistors," *Semi-cond. Sci. Technol.*, vol. 11, pp. 759–765, 1996.

- [2] D. Pan, E. Towe, and S. Kennerly, "A five-period normal-incidence intersubband (In, Ga)As/GaAs quantum dot infrared photodetectors," *Appl. Phys. Lett.*, vol. 75, pp. 2719–2721, 1999.
- [3] S. Kim, H. Mohseni, M. Erdtmann, E. Michel, C. Jelen, and M. Razeghi, "Growth and characterization of InGaAs/InGaP quantum dots for midinfrared photoconductive detector," *Appl. Phys. Lett.*, vol. 73, pp. 963–965, 1998.
- [4] J. Phillips, P. Bhattacharya, S. W. Kennerly, D. W. Beekman, and M. Dutta, "Self-assembled InAs–GaAs quantum dot intersubband detectors," *IEEE J. Quantum Electron.*, vol. 35, pp. 936–943, June 1999.
- [5] J. W. Kim, J. E. Oh, S. C. Hong, C. H. Park, and T. K. Yoo, "Room temperature far infrared (8–10 μm) photodetectors using self-assembled InAs quantum dots with high detectivity," *IEEE Electron Device Lett.*, vol. 21, no. 7, pp. 329–331, 2000.
- [6] O. Baklenov, Z. H. Chen, E. T. Kim, I. Mukhametzhano, A. Madhukar, F. Ma, Z. Ye, B. Yang, and J. Campbell, "Dark current reduction and operational wavelength shift in normal incidence InAs/GaAs QDIP's through the introduction of AlGaAs layers in the active region of the detector," in *Proc. 58th IEEE Device Research Conf.*, Denver, CO, June 2000, p. 171.
- [7] Z. H. Chen, O. Baklenov, E. T. Kim, I. Mukhametzhano, J. Tie, A. Madhukar, Z. Ye, and J. Campbell, "InAs/Al $_x$ Ga $_{1-x}$ As quantum dot infrared photodetectors with undoped active region," in *Proc. QWIP2000 Workshop: Infrared Physics and Technology*, vol. 42, Dana Point, CA, July 2001, p. 479.
- [8] Z. H. Chen, O. Baklenov, E. T. Kim, I. Mukhametzhano, J. Tie, A. Madhukar, Z. Ye, and J. C. Campbell, "Normal incidence InAs/Al $_x$ Ga $_{1-x}$ As quantum dot infrared photodetectors with undoped active region," *J. Appl. Phys.*, vol. 89, pp. 4558–4563, Apr. 2001.
- [9] S. Y. Wang, S. D. Lin, H. W. Wu, and C. P. Lee, "Low dark current quantum-dot infrared photodetectors with an AlGaAs current blocking layer," *Appl. Phys. Lett.*, vol. 78, pp. 1023–1025, Feb. 2001.
- [10] S. Y. Lin, Y. R. Tsai, and S. C. Lee, "High-performance InAs/GaAs quantum-dot infrared photodetectors with a single-sided Al $_{0.3}$ Ga $_{0.7}$ As blocking layer," *Appl. Phys. Lett.*, vol. 78, pp. 2784–2786, Apr. 2001.
- [11] A. D. Stiff, S. Krishna, P. Bhattacharya, and S. Kennerly, "High-detectivity, normal-incidence, mid-infrared ($\lambda \sim 4 \mu\text{m}$) InAs/GaAs quantum-dot detector operating at 150 K," *Appl. Phys. Lett.*, vol. 79, pp. 421–423, July 2001.
- [12] I. Mukhametzhano, Z. Wei, R. Heitz, and A. Madhukar, "Punctuated island growth: An approach to examination and control of quantum dot density, size, and shape evolution," *Appl. Phys. Lett.*, vol. 75, pp. 85–87, July 1999.
- [13] I. Mukhametzhano, Z. H. Chen, O. Baklenov, E. T. Kim, and A. Madhukar, "Optical and photocurrent spectroscopy studies of inter- and intra-band transitions in size-tailored InAs/GaAs quantum dots," *Phys. Status Solidi (b)*, vol. 224, no. 3, pp. 697–702, Mar. 2001.

Zhengmao Ye received the B.S. and M.S. degrees in physics from Nanjing University, Nanjing, China, in 1994 and 1997, respectively, and the M.E. degree in electrical engineering from the University of Texas at Austin in 2000, where he is currently working toward the Ph.D. degree in electrical engineering.

His research includes design, fabrication, and characterization of quantum-dot infrared photodetectors.

Mr. Ye is a student member of the IEEE Lasers and Electro-Optics Society (LEOS).

Joe C. Campbell received the B.S. degree in physics from the University of Texas at Austin in 1969 and the M.S. and Ph.D. degrees from the University of Illinois at Urbana-Champaign in 1971 and 1973, respectively.

From 1974 to 1976, he was with Texas Instruments Incorporated, where he worked on integrated optics. In 1976, he joined the staff of AT&T Bell Laboratories, Holmdel, NJ, where he worked on a variety of optoelectronic devices, including semiconductor lasers, optical modulators, waveguide switches, photonic integrated circuits, and photodetectors with emphasis on high-speed avalanche photodiodes for high-bit-rate lightwave systems. In 1989, he joined the faculty of the University of Texas at Austin as Professor of Electrical and Computer Engineering. He also serves as a Cockrell Family Regents Chair in Engineering. His research interests include Si-based optoelectronics and high-speed photodetectors.

Dr. Campbell was elected a member of the National Academy of Engineering in 2002, in recognition of his contributions to the development of high-speed, low-noise avalanche photodiodes.

Zhonghui Chen received the B.S. degree in semiconductor physics and devices from Nanjing University, Nanjing, China, in 1991. He studied semiconductor physics and optoelectronics at Shanghai Institute of Technical Physics, Chinese Academy of Sciences, Shanghai, China, during 1991–1995, and received the Ph.D. degree in semiconductor materials and surface science from Wuerzburg University, Wuerzburg, Bavaria, Germany, in 1999.

From 1999 to 2001, he was a Research Associate with the Nanostructure Materials and Devices Laboratory, Materials Science and Engineering, University of Southern California at Los Angeles. He was appointed Assistant Research Professor in 2001. His interests include semiconductor epitaxial heterostructure materials, devices and processing, semiconductor optical spectroscopy, and surface analysis of semiconductor structure and chemistry.

Eui-Tea Kim received the B.S. and M.S. degrees in materials engineering from Chungnam National University, Taejon, Korea, in 1991 and 1993, respectively. He is currently working toward the Ph.D. degree in materials science at the University of Southern California at Los Angeles.

He joined the Semiconductor R&D Center, Korea Electronics Co., Ltd., Kyung Ki Do, Korea, where he was a Senior Research Engineer, developing photoconductive and photovoltaic HgCdTe infrared detectors and a high-voltage transistor ($V_{CBO} > 1500$ V) having glass-passivated mesa. His current research involves MBE growth and characterization of InAs quantum-dot infrared photodetectors.

Anupam Madhukar graduated from Lucknow University, Lucknow, India, in 1966, and received the Ph.D. degree in materials and science and physics from the California Institute of Technology, Pasadena, in 1971.

He was with IBM T.J. Watson Research Center, Yorktown Heights, NY, and the James Frank Institute, University of Chicago, Chicago, IL, before joining the University of Southern California at Los Angeles, where he has been Professor of Materials Science and Professor of Physics since 1984. He was appointed the Kenneth T. Norris Professor of Engineering in 1996. His research areas include experimental and theoretical studies of quantum-confined nanostructures, epitaxial growth, *in-situ* process monitoring, large-scale computer simulations of materials and growth, and semiconductor electronic and optoelectronic device applications in information processing.